IMPLEMENTING INNOVATIVE SEA STATE MONITORING SYSTEM BASED ON MICROSEISM

Alfio Marco Borzì[1], Vittorio Minio[2], Raphael De Plaen[3], Thomas Lecocq[3], Flavio Cannavò[2], Giuseppe Ciraolo[4], Sebastiano D'Amico[5], Carlo Lo Re[6], Carmelo Monaco[1,2], Gabriele Nardone[6], Marco Picone[6], Giovanni Scardino[7], Giovanni Scicchitano[7], Francesco Panzera[1], Andrea Cannata[1,2].

Medicanes (Mediterranean hurricanes) and common Mediterranean storms represent substantial hazards to the densely populated coastal regions of the Mediterranean. Both types of events result in significant meteo-marine phenomena such as heavy rainfall, extreme winds, and substantial sea surges, with the potential to cause extensive damage to infrastructure and ecosystems. This study investigates the seismic signatures of these meteorological events, focusing on how continuous seismic noise generated by ocean-solid Earth interactions (microseism) can be used for sea state monitoring and cyclone tracking. The main findings of our work reveal specific spectral characteristics associated to medicanes and common storms. Our approach offers a complementary monitoring system, to be implemented and developed in the coming years for coastal monitoring purposes in complement with other instruments specifically developed for sea state monitoring.

Keywords: microseism; sea state monitoring; medicanes

1. INTRODUCTION

Extreme meteorological events are increasingly affecting the Mediterranean areas with two huge alluvial events that affect Valencia (Spanish) and Giarre-Riposto (Catania, Italy) areas during October and November 2024 (Grau-Bove et al., 2024;). Less recently, the Mediterranean Sea has been affected by several Mediterranean Hurricanes (hereinafter Medicanes) able to generate heavy rain, strong wind gusts, and storm surges with significant wave heights (hereafter SWH) greater than 3 meters. A medicane can be considered a small-scale tropical cyclone that develops in the Mediterranean Sea and usually can reach category one on the Saffir-Simpson hurricane wind scale (Miglietta and Rotunno 2019).

Growing concerns about monitoring extreme meteo-marine events (like Medicanes) are driving the scientific community toward developing complementary sea-state monitoring systems to be added to the commonly used sea-state monitoring systems (i.e. wave-buoys, HF radar). Several authors (Bromirski et al., 1999; Cutroneo et al., 2021; Ferretti et al., 2013, 2018; Minio et al., 2023) analyzed a continuous seismic signal, able to provide information about the sea state. This seismic signal, called microseism, is generated by the interaction between the sea waves and the solid Earth (e.g., Hasselmann, 1963; Longuet-Higgins, 1950). Based on spectral characteristics and source mechanisms (e.g., Haubrich and McCamy, 1969), the microseism can be classified into primary (PM), secondary (SM), and short-period secondary (SPSM) bands. The PM band has the same period as ocean waves (13–20 seconds) and arises from oceanic wave forces on the seafloor in coastal and near-coastal areas with depths less than several hundred meters (Hasselmann, 1963; Ardhuin et al., 2015). The SM band generally exceeds the PM by 10 to 20 dB (Lepore and Grad, 2018; Longuet-Higgins, 1950; Oliver and Page, 1963; Ardhuin et al., 2012, 2015) and results from opposing sea waves that create (mainly Rayleigh) seismic waves at frequencies approximately double that of the originating ocean waves (5–10 seconds). The SPSM band has periods shorter than 5 seconds and is generated by the interaction of local wave movements near the shore (Bromirski et al., 2005). As above mentioned, several works analyzed the relationship between microseism and sea conditions (Ardhuin et al., 2019; Aster et al., 2008, 2010, 2023; Bromirski et al., 1999; Cannata et al., 2019, 2020; Cutroneo et al., 2021) and microseism and cyclonic activity (Bromirski, 2001; Bromirski et al., 2005; Gerstoft et al., 2006; Gualtieri et al., 2018; Lin et al., 2017; Retailleau and Gualtieri, 2019, 2021; Zhang et al., 2010). Bromirski et al. (1999) is the first work that uses microseism to predict the SWH. This study developed an empirically derived seismic-to-wave transfer function, suitable for the California coast, able to predict the SWH. Gerstoft et al. (2006) instead used a seismic array to track the space-time evolution of Hurricane Katrina. These two works demonstrate the possibility of using microseism both to develop a sea state monitoring system and to track, in quasi-real-time, the cyclones' position.

[1]Dipartimento di Scienze Biologiche, Geologiche ed Ambientali - Sezione di Scienze della Terra, Università degli Studi di Catania, Catania, Italy;
[2]Istituto Nazionale di Geofisica e Vulcanologia - Sezione di Catania, Osservatorio Etneo, Catania, Italy;
[3]Seismology-Gravimetry, Royal Observatory of Belgium, Brussel, Belgium;
[4]Dipartimento di Ingegneria, Università degli Studi di Palermo, Bd. 8, 90128 Palermo, Italy;
[5]Department of Geosciences, University of Malta, MSD 2080 Msida, Malta;
[6]Italian Institute for Environmental Protection and Research (ISPRA), via Vitaliano Brancati 48, 00144 Rome, Italy;
[7]Dipartimento di Scienze della Terra e Geoambientali, Università degli Studi di Bari Aldo Moro, 70125 Bari, Italy.

In this work, we analyzed the microseism data recorded during Medicanes and more common seasonal storms to investigate possible microseism feature differences.

2. METEOROLOGICAL EVENTS

In this work, we take into account one Medicane (Apollo), one sub-tropical system (Helios), and one more common seasonal storm (N1). See **Table 1** for details.

Table 1. Date of the events taken into account and features of the microseism source during the day when each event reaches the maximum intensity and Significative R^2 values obtained by performing 20 runs by randomly shuffling the RMS amplitude values among the stations used in the grid search analysis

Name	Date	Latitude (°)	Longitude (°)	R^2	Significative R^2
Helios	9-11/02/2023	36.0348	14.3030	0.51	0.27
Apollo	25/10-02/11/2021	36.3742	14.5857	0.48	0.33
N1	10-12/02/2015	37.0484	16.4560	0.25	0.32

2.1. Medicane Apollo

The Medicane Apollo formed on 25 October 2021, near the Libyan coast as a depression vortex. As it moved northward, the vortex intensified due to the high temperatures of the Mediterranean Sea, eventually developing the characteristics of a Medicane by 28 October. The impacts of Medicane Apollo were especially pronounced around Catania, where an average rainfall of approximately 200 mm over 48 hours was recorded, peaking at 448 mm/48 hours as measured by the Sicilian Meteorological Service ("Regione Siciliana—SIAS—Servizio Informativo Agrometeorologico Siciliano") near Linguaglossa. In the Siracusa area, rainfall surpassed 200 mm on October 29, as reported by the SIAS. The highest wind gusts, reaching 104 km/h, were also recorded on this date, with the minimum atmospheric pressure estimated at 999 hPa (Borzì et al., 2022; Faranda et al., 2022). Sea wave activity intensified as well, with SWH exceeding 3 meters, as observed by the ISPRA buoy located near Crotone (Borzì et al., 2022). Following the Medicane Apollo's transition, the Sicilian regional government declared a state of emergency for 32 municipalities across the provinces of Catania, Messina, Siracusa, and Ragusa, which were the hardest hit by the storm. The damage caused by Apollo was estimated at approximately 2 million euros for emergency response efforts and around 50 million euros for impacts on agriculture, businesses, and infrastructure. Notably, infrastructure damage included sections of the Catania-Siracusa highway due to the overflow of the Simeto River, as well as damage to port facilities caused by intense wave action (Borzì et al., 2022).

2.2. Sub-tropical system Helios

During the period 9-11 February 2023, a low-pressure system, later named Helios, developed over the Sicily Channel due to the sharp contrast between very cold air from the northeast (the Balkans) and the relatively warm sea surface. Satellite data revealed a warm core anomaly within this cyclone, a key feature for Medicane formation. However, Helios did not fully transition into a Medicane, as it lacked the well-developed convection around its eye, likely due to limited interaction between the sea and air resulting from sea surface temperatures unsuitable for Medicane development (Borzì et al., 2024a; D'Adderio et al., 2023; Kushabaha et al 2024; MedCyclones, 2023a, b, c).

Despite not becoming a Medicane, Helios, due to its proximity to the Sicilian and Maltese coasts, caused notable damage in these areas. Its effects were most significant in the southeastern Sicilian provinces of Catania, Ragusa, and Siracusa. The Sicilian meteorological service ("Regione Siciliana–SIAS–Servizio Informativo Agrometeorologico Siciliano") recorded (i) intense rainfall exceeding 200 mm over 48 hours, with peaks around 500 mm over 48 hours near Noto (9-10 February 2023), (ii) heavy snowfall starting from 1200 meters above sea level, with fresh snow accumulations over 2 meters deep on Mount Etna, (iii) strong wind gusts reaching 90 km/h along exposed coastlines (Davies, 2023), and (iv) severe storm surges with SWH exceeding 5 meters. Similar conditions were also observed in Malta, with the cyclone’s minimum pressure reaching 1002 hPa.

In response to the damage caused by Helios, the Sicilian regional government requested a 12-month state of emergency for all municipalities in the provinces of Catania, Siracusa, and Ragusa, as well as some municipalities in the Messina province (Delibera di Giunta – Regione Siciliana, 2023).

2.3. Common Storm

In addition to the previously discussed cyclonic events, this study also examines a common storm that occurred from 10–12 February 2015 (hereafter referred to as N1; Borzì et al., 2024b).
Such common storms are typically associated with baroclinic instability, which arises from the combined effects of air pressure variations and wind stress. These storms often cause temporary sea-level rises due to the inverse barometric effect and the displacement of the water column driven by wind stress, leading to coastal flooding (Doodson, 1923; Lionello and Sanna, 2005; Lionello et al., 2006; Lionello, 2012).
For eastern Sicily, the primary impacts were not due to rainfall but to sustained wind gusts, which reached speeds of approximately 70 km/h. These winds contributed significantly to the storm surge, resulting in coastal flooding.
Although the storm had a relatively limited spatial and temporal impact on the eastern Sicilian and western Greek coastlines in terms of damage, detailed information about its effects is scarce. Wave data, specifically SWH, were obtained from hindcast maps provided by the Copernicus product MEDSEA_HINDCAST_WAV_006_012. Wind gust information was sourced from the website "earth: a global map of wind, weather, and ocean conditions" (https://earth.nullschool.net/, last accessed 18/11/2024).

3. DATA AND METHODS

For all the meteorological events considered in this study, we selected the analysis period to encompass the full lifecycle of each event. This includes the development phase, the peak intensity characterized by the minimum pressure value (specifically for the Medicanes), maximum wind velocity, highest precipitation intensity and SWH, as well as the subsequent weakening phase.

3.1. Seismic Data

We used about 100 seismic stations (Figure 1) located along the Italian coastal areas, including the Sicily Channel coastlines (Malta, Lampedusa, and Linosa islands), Corsica, and the coastal areas of Greece and France. There is no seismic data available from North Africa, and this may affect the quality of some locations.

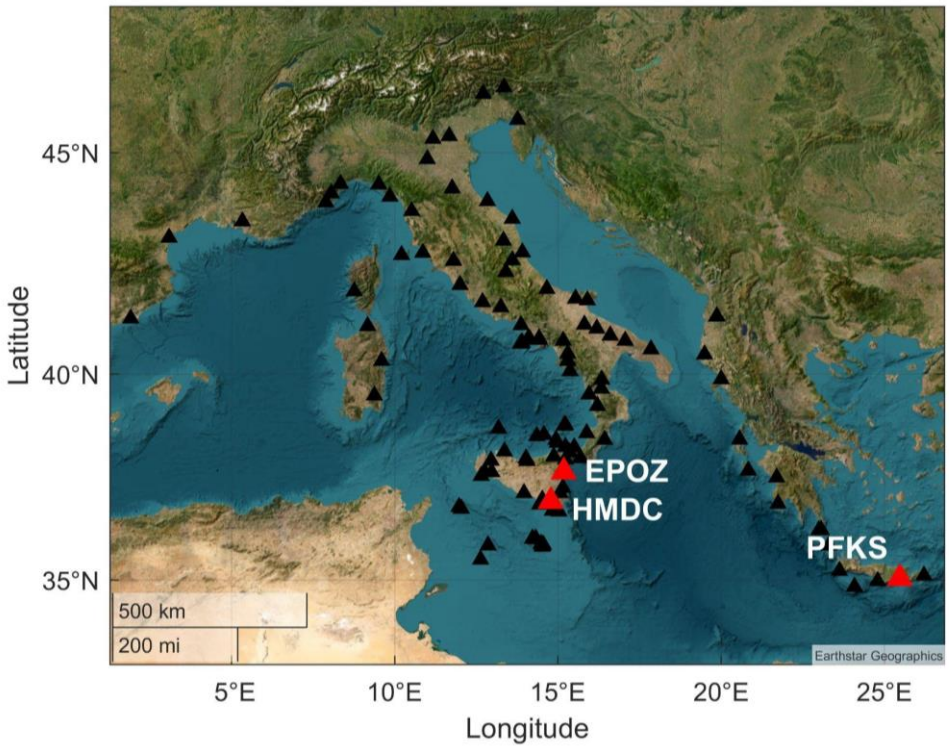

Figure 1. Satellite image of the Mediterranean region with broadband seismic stations (black triangles) used in our analysis. (base image source ©Earthstar Geographic).

The seismic stations were selected based on specific criteria: (i) installation in coastal areas and (ii) configuration with three-component broadband seismic sensors. Data acquisition was conducted at a sampling rate of 100 Hz. It is worth noting that the number of available seismic stations for each event varied slightly due to station malfunctions or differences in installation dates.

3.2. Seismic Analysis

3.2.1. Spectral and amplitude analysis

The seismic data were corrected for instrument response, followed by spectral and amplitude analyses. For the spectral analysis, the seismic signals were processed using Welch's method (Welch, 1967), employing time windows of 81.92 seconds, which facilitated the calculation of hourly spectra. The resulting hourly spectra were compiled and visualized as spectrograms, with time represented on the x-axis, frequency on the y-axis, and the logarithm (base 10) of the power spectral density (PSD) shown on a color scale.

Examples of spectrograms for the vertical component of the EPOZ, PFKS, and HMDC stations are illustrated in Figure 2 for all the events taken into account in this study.

For amplitude analysis, hourly time series of root mean square (RMS) amplitudes were calculated for the 0.1–0.2 Hz frequency band that corresponds to the secondary microseisms (SM, black line in Figure 2).

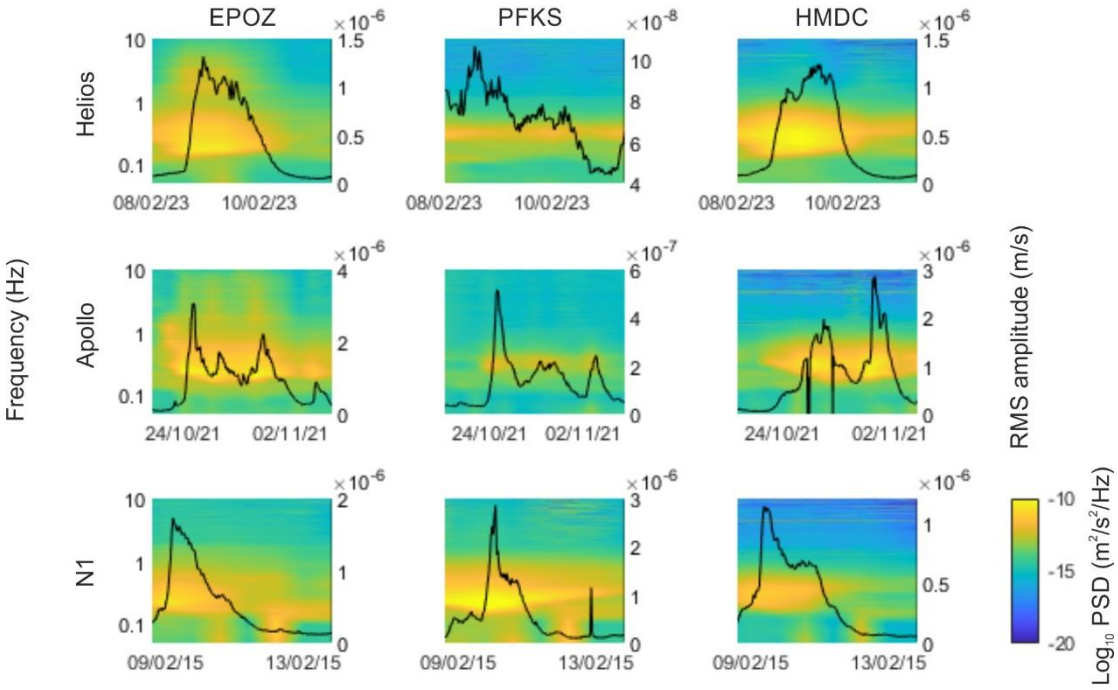

Figure 2. Spectrograms and RMS amplitude time series for the SM band (0.1–0.2 Hz) of the seismic signal recorded by the vertical component of 3 stations located along the Sicilian (EPOZ and HMDC) and the Greek (PFKS) coastlines during the 3 events taken into account. See Figure 1 for the station locations.

3.2.2. Tracking cyclone position

Since microseism is a continuous seismic signal, traditional techniques that rely on the first phase arrivals to localize a seismic event's hypocenter cannot be applied. Consequently, we utilized alternative methods to localize the microseism source, such as a grid search method, based on the decay of seismic amplitudes.

This method assumes that seismic waves propagate through a homogeneous medium (Cannata et al., 2013). The microseism amplitude is modeled as proportional to r^{-b}, where r is the source-station distance, and b represents the geometrical spreading factor, with values of 1 for body waves or 0.5 for surface waves. The b parameter was left unconstrained during the location process. Intrinsic attenuation was accounted for using a frequency-dependent absorption coefficient α in the range of 0–0.25x10^{-3} km^{-1} (Mitchell, 1995).

The microseism source, located on the Earth's surface, was searched using a planar 2D grid (rather than a 3D grid used for volcanoes; Cannata et al., 2013) covering an area of 1610 × 2700 km (spanning longitudes 5° to 27° and latitudes 32° to 46°) with 0.5° spacing. Locations were calculated every 4 hours. The accuracy of this method relies on the R^2 value, representing the linear regression fit for each grid node. The source is positioned at the centroid of nodes with R^2 values within 1% of the maximum. To evaluate reliability, statistical significance was tested by performing 20 random shuffles of RMS amplitude data among stations, calculating the 99th percentile of R^2, as summarized in Table 1.
This method has some limitations. It assumes the microseism source is point-like, whereas microseisms are generated over broad areas. Thus, the identified source represents the barycentric point of the extended source. When multiple sources of similar intensity exist within the same frequency range, the calculated source may shift between actual locations, lowering R^2 (Battaglia et al., 2005). To ensure reliability, we discarded locations with R^2 values below the thresholds in Table 1 for each event.

3.2.3. Seismic signature of cyclones and common storm

To analyze the seismic signature and spectral characteristics of Medicanes and common storms, we applied a method developed by Soubestre et al. (2018). Originally designed for detecting and classifying seismo-volcanic tremors, this network-based approach utilizes the coherence of tremor signals across a network, estimated through the array covariance matrix. This technique identifies spatially coherent noise sources, such as volcanic tremors, tectonic earthquakes, and oceanic seismic noise (microseisms), while distinguishing them from localized noise, which generates multiple sources with broader spectral widths. In this study, the method was used to examine the spectral content of cyclones and common storms to determine whether their spectral characteristics are similar or different.
Focusing on microseism noise, the seismic signals were filtered in the 0.1–1 Hz frequency band and resampled at 25 Hz to optimize computational challenges.
Only the vertical component of the seismic signal was used, with a 60-second window length for calculating the covariance matrix.

3.2.4. Seismic strength of Medicanes and common storm

Several studies have sought to estimate the seismic intensity of tropical cyclones using various approaches. Gualtieri et al. (2018) proposed a two-step method to estimate cyclone intensity from ambient seismic noise. First, they developed a generalized linear model (GLM) linking tropical cyclone intensity to the PSD of seismic noise using data from 2000–2010. Then, they used this model to predict cyclone intensity for 2011–2012, demonstrating a correlation between cyclone intensity (derived from meteorological data) and increases in the PSD of primary, secondary, and short-period secondary microseisms.
For this study, we applied a similar approach to calculate the Microseism Reduced Amplitude (MRA) for the two cyclonic events and for the common storm. The MRA at each seismic station was computed using the equation:
$MRA = RMS \times d$ (eq.1)
where d is the source-station distance (meters), derived from localization analysis based on seismic amplitude decay (assuming the cyclone as a point-like source), and RMS is the recorded amplitude (m/s) for the SM band at that station during the relevant time interval.
The MRA of each cyclone was calculated only for periods when localization was deemed reliable. To determine a single representative seismic amplitude for each cyclone, we tested seven station selection methods: i) the 30 stations nearest to the source, ii) the 40 stations nearest to the source, iii) the 50 stations nearest to the source, iv) stations within 300 km of the source, v) stations within 400 km of the source, vi) stations with RMS amplitudes smaller than the station nearest the source, vii) all 105 stations. Methods involving a 300 or 400 km radius were excluded due to limited station coverage (3–4 stations for some Medicanes). Since the remaining methods yielded similar results, we selected all the stations to ensure consistency and calculated the median MRA value as the seismic amplitude at the source for each event.
For the common storm, which affected larger areas of the Ionian Sea and the grid search method did not provide reliable results, the storm's source was defined as the centroid of the region with SWH>3 m, as determined from hindcast maps. This approach allowed us to compute and compare the MRA of common storms with that of cyclones.

4. RESULTS AND DISCUSSIONS

In this work, we analyzed the features of microseism during a Medicane, a sub-tropical system, and a common storm that occurred in the Mediterranean area between February 2015 and February 2023. In detail, we performed spectral and location analysis and retrieved the seismic signature and the MRA for the three aforementioned events.

4.1. Spectral, amplitude and location analysis

In this section, we present and discuss the results of the spectral and location analysis performed for the two cyclonic events and the common storm taken into account. Borzì et al. (2022) showed that the microseism band mostly showing the cyclonic effects is the SM. Hence, we use the SM band to track the position of the two cyclonic events analyzed in this work, similarly, spectral and amplitude analysis has been performed for the SM band.

4.1.1. Apollo

Apollo was the most recent Medicane, forming in the Ionian Sea in late October 2021. Spectrograms and RMS amplitude time series (Figure 2), obtained for the three seismic stations considered, clearly show its evolution, peak intensity (that occurred on 29 October 2021), and subsequent weakening. Regarding the localization analysis, Medicane Apollo was tracked throughout the entire day of 29 October 2021 (example shown in Figure 3a). In detail, we obtained source locations that aligned with the Medicane's position in the Ionian Sea and additionally, by performing one localization every four hours, we were able to track Apollo's movement. Specifically, we obtained the first significant location on 29 October at 04:00. From that point, we were able to track Apollo's northward shift until 20:00 on 29 October. For the entire day on 30 October, we followed the southward movement of the Medicane. The results obtained by using this method were consistent with the actual change of positionof the Medicane.

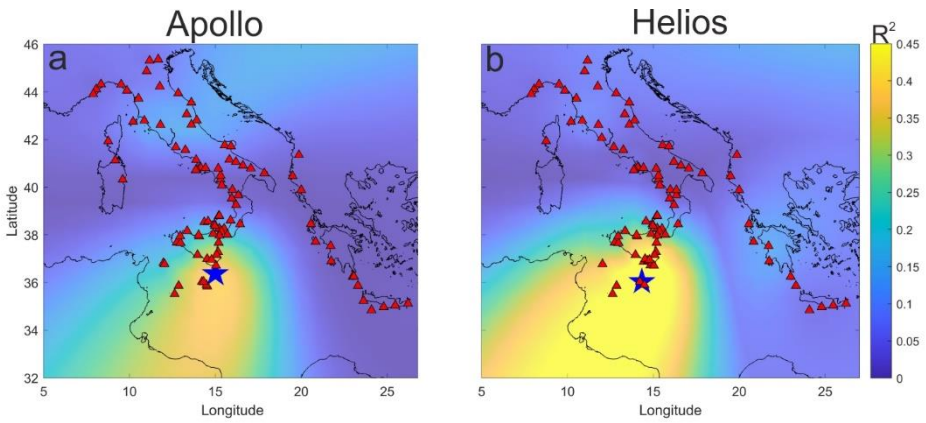

Figure 3. Localization of the microseism source for the days when each event reaches its climax. The blue five-point star indicates the centroid position of all the grid nodes whose R^2 values do not differ by >1 % from the maximum R^2 value obtained with the grid search method.

4.1.2. Helios

Helios was a sub-tropical system forming in the Sicily channel during February 2023. As in the Apollo case, spectrograms and RMS amplitude time series (Figure 2), especially for the stations EPOZ and HMDC, show the development, the climax, and the subsequent loss of power of this event. Concerning the localization analysis, we obtained reliable locations from 08:00 on 9 February 2023, to 00:00 on 11 February 2023. According to satellite data, Helios was not yet fully developed on 9 February 2023 and did not display a well-formed cyclone eye. However, on this day, we were able to identify a storm surge, likely related to the initial formation of Helios, in the Ionian Sea. Specifically, our localizations from 08:00 to 20:00 on 9 February indicated the source position near southeastern Sicily, consistent with hindcast data showing SWH greater than 5 meters in this area. Over the following hours, our localizations revealed a small but steady shift of the source towards the Malta area, in agreement with the relatively stable position of the cyclone eye during the early hours of 10 February 2023 (Figure 3b), as seen in

satellite data. The subtropical system then rapidly weakened and dissipated completely by 11 February 2023, making landfall against the Libyan coast.

4.1.3 Common Storm N1

We also analyzed a common storm called N1 to understand if this storm presents similar or different features compared with the Medicane and the sub-tropical system. The spectrograms and RMS amplitude time series (Figure 2) show a good agreement with the development of the storms. In particular, it is possible to see that the Greek station recorded the maximum PSD and RMS amplitude with a delay compared with the Sicilian stations. This aspect results in agreement with the eastward movement of the storm. Additionally, we try to locate this common seasonal storm by using the grid search method, but, while obtaining localizations in agreement with the real positions of the storms, the R2 values turn out to be lower than the reliable R2 threshold (Table 1). Indeed, these storms simultaneously affect distant and large areas. For instance, the Sicilian, Calabrian, Apulian, Maltese, African, and Greek coastline were affected by the N1 storm, hence every one of these areas can be considered as a source. We are therefore in the case of multiple sources that, as explained in the Data and Methods section, invalidate our localization assumptions.

4.2. Seismic Signature of cyclones and common storm

We employed the covariance matrix method primarily to examine the seismic spectral content of the Medicane, the subtropical system, and the common storm. This approach allowed us to exclude local noise sources and effects, enabling a meaningful comparison of the spectral characteristics among these phenomena. In Figure 4, we show the results of the covariance matrix during cyclonic events (Figure 4a and b) and the common storm (Figure 4c).

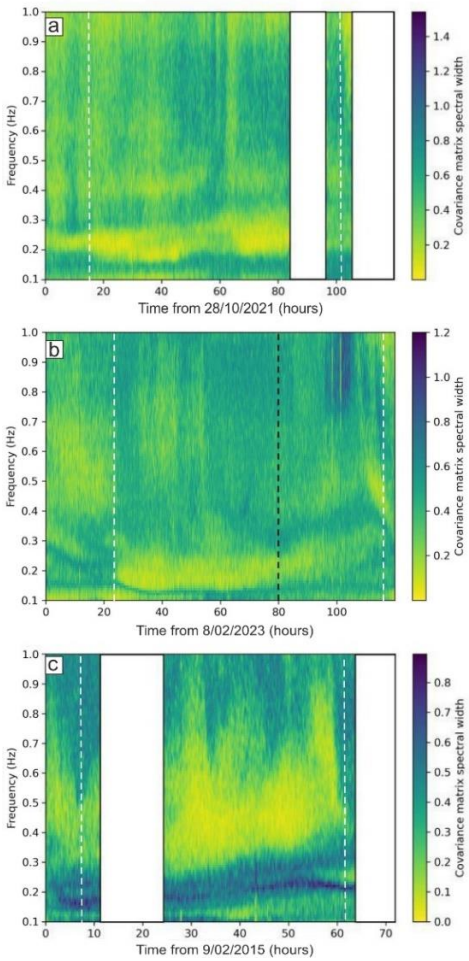

Figure 4. Covariance matrix obtained for the Medicane Apollo (a), Sub-tropical system Helios (b) and common storm N1 (c).

The analysis revealed some differences in the spectral content between cyclonic events and common storms. Specifically, Medicanes like Apollo (Figure 4a) and subtropical systems such as Helios (Figure 4b) exhibited well-defined microseism spectral characteristics in the SM and SPSM frequency bands (0.18–0.35 Hz). In contrast, common storms displayed a broader and higher spectral content, ranging from 0.3 to 0.7 Hz.

As previous studies on microseisms and tropical cyclones have shown (e.g., Gerstoft et al., 2006; Gualtieri et al., 2018; Lin et al., 2017; Retailleau and Gualtieri, 2019; Zhang et al., 2010), the spectral signature of Medicanes (0.18–0.35 Hz) indicates that all rotating and moving cyclonic systems, including Medicanes and smaller subtropical events like Helios, can generate microseisms in these bands. In particular, the interaction between different wave systems located around the cyclone corresponds to the SM definition.

For common storms (Figure 4c), the broader and higher spectral range appears to result from the extensive area affected by these storms. While Medicanes are more intense meteorological events, their influence is limited to a relatively small area (100–300 km in diameter, on average), this allows us to consider these events as a point-like source. In contrast, common storms impact the entire Mediterranean Sea over their lifespan. For example, an Atlantic storm may first affect the Tyrrhenian Sea and western Italy with heavy rainfall, then move to the Ionian Sea and eastern Italy, producing strong wind gusts of 50–70 km/h. These widespread effects classify common storms as extended sources rather than point-like ones.

The wider extent of the affected area and the absence of strong rotational dynamics around a pressure minimum in common storms help explain their higher and broader spectral content. This difference also accounts for the lack of high coherence values for frequencies below 0.3 Hz, indicating that common storms are less efficient in generating SM but can efficiently generate SPSM through local wave motions near coastlines.

The higher frequencies (above 0.3 Hz) observed during common storms are likely associated with interactions between shorter-period waves (less than 6 seconds), common in the Mediterranean Sea during these events (Agenzia per la Protezione dell'Ambiente e per i Servizi Tecnici- Atlante delle onde nei mari Italiani). These waves cause pressure fluctuations that propagate from the sea surface to the seabed, and their interactions in varied sea depths across the wide area affected by common storms amplify this spectral content. In a semi-enclosed basin like the Ionian Sea, such interactions, combined with coastal reflections, can lead to resonance effects. For instance, during common storms, Italian wave buoy data show that wave periods predominantly range from 3 to 7 seconds, with the most frequent periods between 3 and 5 seconds. Conversely, extreme events like Medicanes are associated with longer wave periods, typically 8–10 seconds, as seen in hindcast data (Atlante delle onde nei mari Italiani https://www.isprambiente.gov.it/it/pubblicazioni/rapporti/atlante-delle-onde-nei-mari-italiani). The interaction of shorter-period waves in coastal areas, as described for PM, SM, and SPSM, contributes to the generation of higher-frequency microseisms during common storms.

In the case of Helios, the subtropical system, a notable frequency variation over time was observed. This change can be attributed to variations in sea depth, consistent with findings in the literature (Gerstoft et al., 2006; Sun et al., 2013), which demonstrate that microseism frequency is influenced by sea depth. For example, Gerstoft et al. (2006) reported frequency increases during Hurricane Katrina's landfalls, and Sun et al. (2013) documented similar patterns for typhoons nearing land. Likewise, on February 11, we observed a frequency increase for Helios, the only system in our study to make landfall (on the Libyan coast). In contrast, Apollo, which did not approach land, showed a stable spectral trend without significant frequency changes.

4.3. Seismic Strength of cyclones and common storm

To assess the strength of Medicanes, sub-tropical systems, and common storms from a seismic perspective, we employ the MRA equation (Eq. 1) detailed in the Data and Methods section. This analysis yields two main findings. First, cyclone events and common storms exhibit significantly different MRA values. Second, for both event types, the MRA is strongly correlated with the size of the sea area where the SWH exceeds 3 meters.

Table 2. Main meteorological parameters of the three events taken into account and results of the MRA analysis.

Name	Rain (mm)	Max Wind Gust (km/h)	SWH (m)	Minimum Pressure (hPa)	Duration (days)	Area (km^2) with SWH > 3 m	MRA (m^2/s)
Helios	>200	90	>5	1002	3	5.92E+05	0.0924
Apollo	>200	104	>4	999	4	1.61E+05	0.0403
N1	/	65	>3	/	3	7.11E+05	0.6683

Table 2 summarizes key meteorological parameters and the results of the MRA analysis for the three studied events.

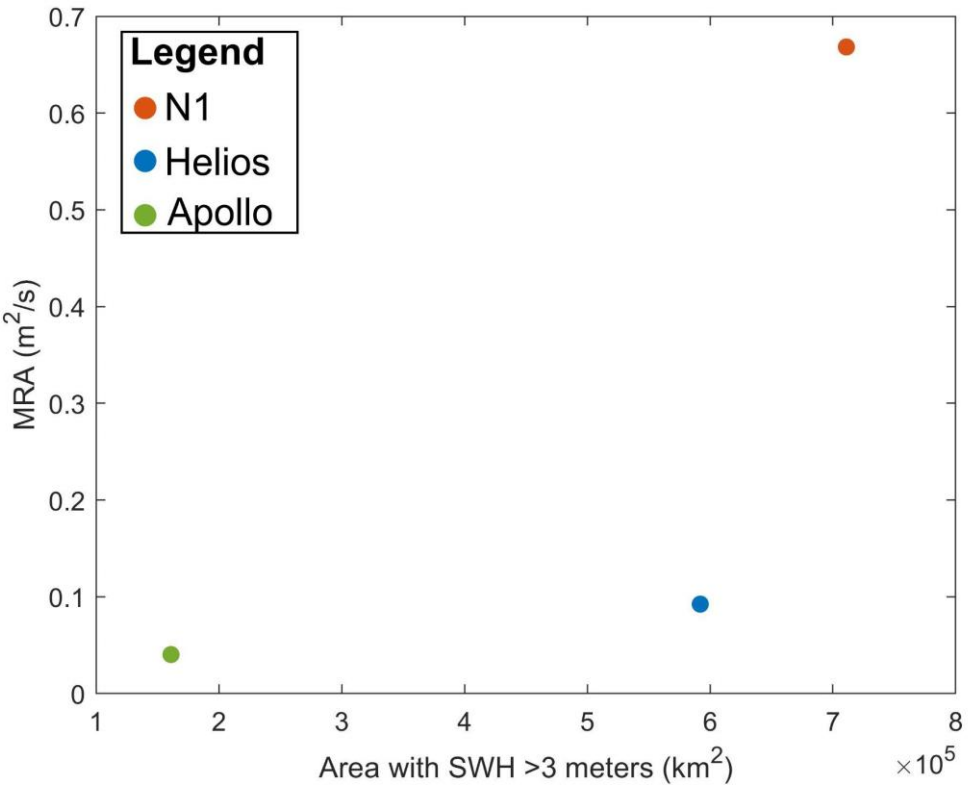

Figure 5. Scatter plot showing the MRA values in the y-axis and the area affected by SWH >3 m in the x-axis both for the three events taken into account.

Comparing the MRA values with various meteorological parameters, it becomes evident that the extent of the sea area with SWH > 3 m significantly influences the MRA, whereas other meteorological parameters appear less relevant to this analysis (see Table 2 and Figure 5). In particular, Figure 5 and Table 2 demonstrate that an increase in the sea area with SWH > 3 m corresponds to a higher MRA across all the considered events. The SWH > 3 m threshold was selected because it marks the point where the correlation between microseism energy (RMS and PSD) and sea state becomes apparent.
For instance, the maximum MRA value, 0.6683 m^2/s, was recorded for the common storm N1, which affected the largest sea area with SWH > 3 m (7.11×10^5 km^2). Conversely, the minimum MRA value,

0.0403 m^2/s, was observed for the Medicane Apollo, which impacted the smallest sea area with SWH > 3 m (1.61×10^5 km^2).
Although MRA is clearly linked to the extent of the area with SWH > 3 m for both types of events, the relationship differs quantitatively. For a comparable sea area extent, the MRA values for common storms are higher than those for cyclone events. For example, the sub-tropical system Helios and the common storm N1 both exhibit similar areas with SWH > 3 m, but their MRA values are 0.0924 m^2/s and 0.6683 m^2/s, respectively. This suggests that energy transfer between sea waves and the solid Earth is more efficient during common storms than during Medicanes.
In cyclones, the generation of secondary microseisms (SM) is influenced by the rotational motion around the cyclone's eye, which produces opposing waves of similar frequency (Lin et al., 2017). By contrast, in common storms, the lack of a defined storm center, the extensive sea area affected, and the quasi-enclosed nature of the Mediterranean Sea may result in multiple uncorrelated wave systems. According to Ardhuin et al. (2019), uncorrelated wave systems generate stronger noise and consequently more intense microseisms.
Comparing the obtained MRA values with several meteorological parameters it is clear that the areal extent of the sea with SWH >3 m influences the MRA, while the other meteorological parameters are not likely to be relevant for this analysis (Table 2 and Figure 5).

5. CONCLUSIONS

This study demonstrates the potential of using microseism analysis as a complementary tool for monitoring extreme meteorological events, such as Medicanes, sub-tropical systems, and common Mediterranean storms. By analyzing the seismic data recorded during three distinct events (Medicane Apollo, sub-tropical system Helios, and the common storm N1), we investigated the spectral characteristics, localization, and seismic strength of these phenomena.

Our findings highlight significant differences in the seismic signatures of cyclonic and non-cyclonic events. While Medicanes and sub-tropical systems generate well-defined secondary microseism (SM) spectral characteristics within specific frequency bands (0.18–0.35 Hz), common storms display a broader spectral range (0.3–0.7 Hz). This distinction is attributed to the larger and more dispersed areas impacted by common storms compared to the more localized nature of cyclonic systems.

Moreover, the reduced amplitude analysis (MRA) revealed a strong correlation between the MRA values and the extent of the sea area with significant wave heights (SWH) exceeding 3 meters. Among the events studied, the common storm N1 exhibited the highest MRA value (0.6683 m^2/s), consistent with its impact on the largest sea area with SWH > 3 m. Conversely, Medicane Apollo, with the smallest affected area, showed the lowest MRA (0.0403 m^2/s). These results suggest that energy transfer from sea waves to the solid Earth is more efficient during common storms than during Medicanes, likely due to the absence of a central storm structure and the presence of uncorrelated wave systems.

The findings of this study highlight the effectiveness of microseism analysis for characterizing meteo-marine phenomena and tracking storms and cyclones. This approach can complement existing monitoring systems, offering valuable insights for coastal hazard assessment and mitigation strategies in the Mediterranean region. Future work should focus on refining microseism-based techniques and integrating them into operational sea-state monitoring frameworks.

ACKNOWLEDGMENTS

The authors thank the ICCE 2024 conference planners. A.M.B. thanks the PON “Ricerca e Innovazione 2014-2020 Azione IV.5 - Dottorati su tematiche green”. This study has been conducted using E.U. Copernicus Marine Service Information, (https://doi.org/10.25423/cmcc/medsea_multiyear_wav_006_012). A.C., G.C., G.S. thank the PRIN 2022 PNRR project titled “ARCHIMEDE - MultidisciplinARy approaCH to better define vulnerabIlity and hazard of MEDicanEs along the Ionian coasts of Sicily” (code P2022MJKMA,

CUP H53D23011380001, E53D23021980001, B53D23033690001, Principal Investigator Prof. G. Scicchitano).

REFERENCES

Agenzia per la Protezione dell''Ambiente e per i Servizi Tecnici Dipartimento Tutela Acque Interne e Marine Servizio Mareografico - Atlante delle onde nei mari italiani - Università degli studi di Roma Tre http://opac.apat.it/sebina/repository/catalogazione/immagini/pdf/atlante%20mari%201_60_2_.pdf

Ardhuin, F., & Roland, A. (2012). Coastal wave reflection, directional spread, and seismoacoustic noise sources. Journal of Geophysical Research: Oceans, 117(C11). https://doi.org/10.1029/2011JC007832

Ardhuin, F., Gualtieri, L., & Stutzmann, E. (2015). How ocean waves rock the Earth: Two mechanisms explain microseisms with periods 3 to 300 s. Geophysical Research Letters, 42(3), 765-772. https://doi.org/10.1002/2014GL062782

Ardhuin, F., Stopa, J. E., Chapron, B., Collard, F., Husson, R., Jensen, R. E., ... & Young, I. (2019). Observing sea states. Frontiers in Marine Science, 124. https://doi.org/10.3389/fmars.2019.00124

Aster, R. C., McNamara, D. E., & Bromirski, P. D. (2008). Multidecadal climate-induced variability in microseisms. Seismological Research Letters, 79(2), 194-202.

Aster, R. C., McNamara, D. E., & Bromirski, P. D. (2010). Global trends in extremal microseism intensity. Geophysical Research Letters, 37(14).

Aster, R. C., Ringler, A. T., Anthony, R. E., & Lee, T. A. (2023). Increasing ocean wave energy observed in Earth's seismic wavefield since the late 20th century. Nature Communications, 14(1), 6984.
Battaglia, J., Aki, K., & Ferrazzini, V. (2005). Location of tremor sources and estimation of lava output using tremor source amplitude on the Piton de la Fournaise volcano: 1. Location of tremor sources. Journal of Volcanology and Geothermal Research, 147(3-4), 268-290.

Borzì, A. M., Minio, V., Cannavò, F., Cavallaro, A., D'Amico, S., Gauci, A., ... & Cannata, A. (2022). Monitoring extreme meteo-marine events in the Mediterranean area using the microseism (Medicane Apollo case study). Scientific Reports, 12(1), 21363.

Borzì, A. M., Minio, V., De Plaen, R., Lecocq, T., Alparone, S., Aronica, S., ... & Cannata, A. (2024a). Integration of microseism, wavemeter buoy, HF radar and hindcast data to analyze the Mediterranean cyclone Helios. Ocean Science, 20(1), 1-20.

Borzì, A. M., Minio, V., De Plaen, R., Lecocq, T., Cannavò, F., Ciraolo, G., ... & Cannata, A. (2024b). Long-term analysis of microseism during extreme weather events: Medicanes and common storms in the Mediterranean sea. Science of the Total Environment, 915, 169989.

Bromirski, P. D., Flick, R. E., & Graham, N. (1999). Ocean wave height determined from inland seismometer data: Implications for investigating wave climate changes in the NE Pacific. Journal of Geophysical Research: Oceans, 104(C9), 20753-20766.

Bromirski, P. D. (2001). Vibrations from the "perfect storm". Geochemistry, Geophysics, Geosystems, 2(7). https://doi.org/10.1029/2000GC000119

Bromirski, P. D., Duennebier, F. K., & Stephen, R. A. (2005). Mid-ocean microseisms. Geochemistry, Geophysics, Geosystems, 6(4). https://doi.org/10.1029/2004GC000768

Cannata, A., Di Grazia, G., Aliotta, M., Cassisi, C., Montalto, P., & Patanè, D. (2013). Monitoring seismo-volcanic and infrasonic signals at volcanoes: Mt. Etna case study. Pure and Applied Geophysics, 170, 1751-1771

Cannata, A., Cannavò, F., Moschella, S., Gresta, S., & Spina, L. (2019). Exploring the link between microseism and sea ice in Antarctica by using machine learning. Scientific reports, 9(1), 13050.

Cannata, A., Cannavò, F., Moschella, S., Di Grazia, G., Nardone, G., Orasi, A., ... & Gresta, S. (2020). Unraveling the relationship between microseisms and spatial distribution of sea wave height by statistical and machine learning approaches. Remote Sensing, 12(5), 761. https://doi.org/10.3390/rs12050761

Cutroneo, L., Ferretti, G., Barani, S., Scafidi, D., De Leo, F., Besio, G., & Capello, M. (2021). Near real-time monitoring of significant sea wave height through microseism recordings: Analysis of an exceptional sea storm event. Journal of Marine Science and Engineering, 9(3), 319.

D'Adderio, L. P., Panegrossi, G., Dafis, S., Rysman, J. F., Casella, D., Sanò, P., ... & Miglietta, M. M. (2024). Helios and Juliette: Two falsely acclaimed Medicanes?. Atmospheric Research, 299, 107179.

Doodson, A. T. (1923). Meteorological Perturbations of Sea-Level.". Nature, 112(2821), 765-766.

Faranda, D., Bourdin, S., Ginesta, M., Krouma, M., Noyelle, R., Pons, F., ... & Messori, G. (2022). A climate-change attribution retrospective of some impactful weather extremes of 2021. Weather and Climate Dynamics, 3(4), 1311-1340.

Ferretti, G., Scafidi, D., Cutroneo, L., Gallino, S., & Capello, M. (2016). Applicability of an empirical law to predict significant sea-wave heights from microseisms along the Western Ligurian Coast (Italy). Continental Shelf Research, 122, 36-42.

Ferretti, G., Barani, S., Scafidi, D., Capello, M., Cutroneo, L., Vagge, G., & Besio, G. (2018). Near real-time monitoring of significant sea wave height through microseism recordings: An application in the Ligurian Sea (Italy). Ocean & Coastal Management, 165, 185-194.

Gerstoft, P., Fehler, M. C., & Sabra, K. G. (2006). When katrina hit california. Geophysical Research Letters, 33(17). https://doi.org/10.1029/2006GL027270

Grau-Bove, J., Higha, R., Orr, S., & Kumar, P. (2024). Short note on the mapping of heritage sites impacted by the 2024 floods in Valencia, Spain. arXiv preprint arXiv:2411.08717.

Gualtieri, L., Camargo, S. J., Pascale, S., Pons, F. M., & Ekström, G. (2018). The persistent signature of tropical cyclones in ambient seismic noise. Earth and Planetary Science Letters, 484, 287-294.https://doi.org/10.1016/j.epsl.2017.12.026

Hasselmann, K. (1963). A statistical analysis of the generation of microseisms. Reviews of Geophysics, 1(2), 177-210. https://doi.org/10.1029/RG001i002p00177

Haubrich, R. A., & McCamy, K. (1969). Microseisms: Coastal and pelagic sources. Reviews of Geophysics, 7(3), 539-571. https://doi.org/10.1029/RG007i003p00539

Kushabaha, A., Scardino, G., Sabato, G., Miglietta, M. M., Flaounas, E., Monforte, P., ... & Scicchitano, G. (2024). ARCHIMEDE—An Innovative Web-GIS Platform for the Study of Medicanes. Remote Sensing, 16(14), 2552.
Lepore, S., & Grad, M. (2018). Analysis of the primary and secondary microseisms in the wavefield of the ambient noise recorded in northern Poland. Acta Geophysica, 66, 915-929.

Lin, J., Lin, J., & Xu, M. (2017). Microseisms generated by super typhoon Megi in the western Pacific Ocean. Journal of Geophysical Research: Oceans, 122(12), 9518-9529. https://doi.org/10.1002/2017JC013310

Lionello, P., & Sanna, A. (2005). Mediterranean wave climate variability and its links with NAO and Indian Monsoon. Climate Dynamics, 25(6), 611-623.

Lionello, P., Malanotte-Rizzoli, P., Boscolo, R., Alpert, P., Artale, V., Li, L., ... & Xoplaki, E. (2006). The Mediterranean climate: an overview of the main characteristics and issues. Developments in earth and environmental sciences, 4, 1-26.

Lionello, P. (Ed.). (2012). The climate of the Mediterranean region: From the past to the future. Elsevier.
Longuet-Higgins, M. S. (1950). A theory of the origin of microseisms. Philosophical Transactions of the Royal Society of London. Series A, Mathematical and Physical Sciences, 243(857), 1-35. https://doi.org/10.1098/rsta.1950.0012

MedCyclones [@MedCyclones_a]: A warm-air seclusion has formed south of #Malta According to GFS the warm core will remain shallow today. Indeed, the absence of deep convection close to the center of the cyclone distinguishes it from #Medicanes. Heavy rainfall and snowfall events will continue to affect #Italy, https://twitter.com/medcyclones/status/1623992335104081921?s=20 (last access: 23 May 2023), X, posted: 11:28, 10 February 2023a.

MedCyclones [@MedCyclones_b]: A nasty warm conveyor belt has covered southern Italy and is associated with a Mediterranean cyclone with a center of minimum MSLP SE of Malta. @meteonetwork weather stations report very high accumulations of rainfall and snow in Sicily on Thu 9/2, https://twitter.com/medcyclones/status/1623795373423620096?s=20 (last access: 23 May 2023), X, posted: 10:26, 9 February 2023b.

MedCyclones [@MedCyclones_c]: A nasty warm conveyor belt has covered southern Italy and is associated with a Mediterranean cyclone with a center of minimum MSLP SE of Malta. @meteonetwork weather stations report very high accumulations of rainfall and snow in Sicily on Thu 9/2, https://twitter.com/medcyclones/status/1624143740800536591?s=20 (last access: 23 May 2023), X, posted: 10:26, 9 February 2023c.

Miglietta, M. M., & Rotunno, R. (2019). Development mechanisms for Mediterranean tropical-like cyclones (medicanes). Quarterly Journal of the Royal Meteorological Society, 145(721), 1444-1460.
Minio, V., Borzì, A. M., Saitta, S., Alparone, S., Cannata, A., Ciraolo, G., ... & Cannavò, F. (2023). Towards a monitoring system of the sea state based on microseism and machine learning. Environmental Modelling & Software, 167, 105781.

Mitchell, B. J. (1995). Anelastic structure and evolution of the continental crust and upper mantle from seismic surface wave attenuation. Reviews of Geophysics, 33(4), 441-462.

Oliver, J., & Page, R. (1963). Concurrent storms of long and ultralong period microseisms. Bulletin of the Seismological Society of America, 53(1), 15-26.

Retailleau, L., & Gualtieri, L. (2019). Toward high-resolution period-dependent seismic monitoring of tropical cyclones. Geophysical Research Letters, 46(3), 1329-1337. https://doi.org/10.1029/2018GL080785

Retailleau, L., & Gualtieri, L. (2021). Multi-phase seismic source imprint of tropical cyclones. Nature communications, 12(1), 2064. https://doi.org/10.1038/s41467-021-22231-y

Soubestre, J., D'Auria, L., Barrancos, J., Padilla, G. D., & Perez, N. (2018, December). Monitoring of Teide volcano (Canary Islands) through a seismic network covariance matrix analysis. In BigSkyEarth Conference: AstroGeoInformatics (p. 15).

Welch, P. (1967). The use of fast Fourier transform for the estimation of power spectra: a method based on time averaging over short, modified periodograms. IEEE Transactions on audio and electroacoustics, 15(2), 70-73.

Zhang, J., Gerstoft, P., & Bromirski, P. D. (2010). Pelagic and coastal sources of P-wave microseisms: Generation under tropical cyclones. Geophysical Research Letters, 37(15). https://doi.org/10.1029/2010GL044288